NANO LETTERS

Letter

pubs.acs.org/NanoLett

In Situ Quantitative Study of Nanoscale Triboelectrification and Patterning

Yu Sheng Zhou,[†] Ying Liu,[†] Guang Zhu,[†] Zong-Hong Lin,[†] Caofeng Pan,[‡] Qingshen Jing,[†] and Zhong Lin Wang*[,†,‡]

[†]School of Materials Science and Engineering, Georgia Institute of Technology, Atlanta, Georgia 30332-0245, United States

[‡]Beijing Institute of Nanoenergy and Nanosystems, Chinese Academy of Sciences, Beijing, China

Supporting Information

ABSTRACT: By combining contact-mode atomic force microscopy (AFM) and scanning Kevin probe microscopy (SKPM), we demonstrated an in situ method for quantitative characterization of the triboelectrification process at the nanoscale. We systematically characterized the triboelectric charge distribution, multifriction effect on charge transfer, as well as subsequent charge diffusion on the dielectric surface: (i) the SiO_2 surface can be either positively or negatively charged through triboelectric process using Si-based AFM probes with and without Pt coating, respectively; (ii) the triboelectric charges accumulated from multifriction and eventually reached to saturated concentrations of (-150 ± 8) $\mu C/m^2$ and (105 ± 6) $\mu C/m^2$, respectively; (iii) the charge diffusion coefficients on SiO_2 surface were measured to be $(1.10 \pm 0.03) \times 10^{-15}$ m^2/s for the positive charge and $(0.19 \pm 0.01) \times 10^{-15}$ m^2/s for the negative charges. These quantifications will facilitate a fundamental understanding about the triboelectric and de-electrification process, which is important for designing high performance triboelectric nanogenerators. In addition, we demonstrated a technique for nanopatterning of surface charges without assistance of external electric field, which has a promising potential application for directed self-assembly of charged nanostructures for nanoelectronic devices.

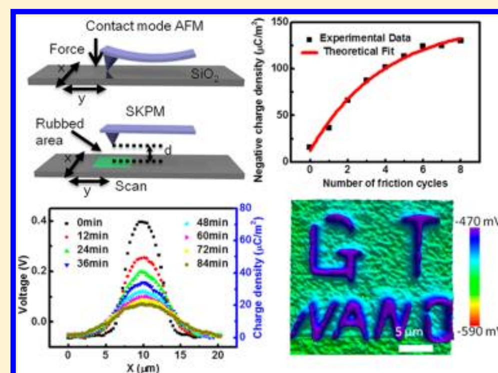

KEYWORDS: *Triboelectric, atomic force microscopy, scanning Kelvin probe microscopy, nanogenerators, TENG*

Charge transfer between surfaces of two distinctly different materials through triboelectric effect is a well-known phenomenon[1−3] that has various applications such as powder spray painting,[4] electrophotography,[5,6] electrostatic separation,[7] and energy harvesting.[8] Recently, triboelectric nanogenerators (TENGs) have been invented for harvesting ambient mechanical energy based on the triboelectric effect coupled with electrostatic effect, and it has demonstrated unprecedented high output of its kind in both voltage and power density and efficiency, showing great promise for building self-powered portable electronics as well as possible large-scale energy harvesting.[9−11]

Although the triboelectrification effect has been known for thousands of years, a fundamental understanding about it is rather limited. Research has been conducted to characterize the triboelectrification process using various methods such as rolling sphere tool-collecting induced charges from rolling spheres on top of a dielectric disk,[12−15] and using atomic force microscopy (AFM) to measure surface electrostatic force or potential on surfaces contacted by micropatterned materials.[16−18] However, these methods either lack an accurate control of the electrification process and/or cannot directly reveal the triboelectric interface, thus hardly achieving a quantitative understanding about the in situ triboelectric process.

Here, we demonstrate an in situ method to quantitatively characterize the triboelectrification at nanoscale via a combination of contact-mode AFM and scanning Kevin probe microscopy (SKPM). Benefitting from the fact that the AFM system can precisely control the contact force, area, speed, and cycles of the triboelectric process, systematical characterizations of the triboelectrification were realized including triboelectric charge distribution, multifriction effect, and the subsequent charge diffusion on the dielectric surface. This methodology provides a powerful tool to investigate the parameters that are important in designing high-performance TENGs. Furthermore, we demonstrated nanopatterning of surface charges using an AFM based triboelectrification process, which has promising applications for directed nanoassembly[19] of charged nanostructures.

Our design for the in situ triboelectric characterization is illustrated in Figure 1a and b. First, the AFM was operated in contact mode under a normal contact force of 120 nN to induce a friction pattern of 4×4 μm^2 area on a silicon oxide film (Figure 1a). Subsequently the surface topography and

Received: March 18, 2013
Revised: April 26, 2013

ACS Publications © XXXX American Chemical Society

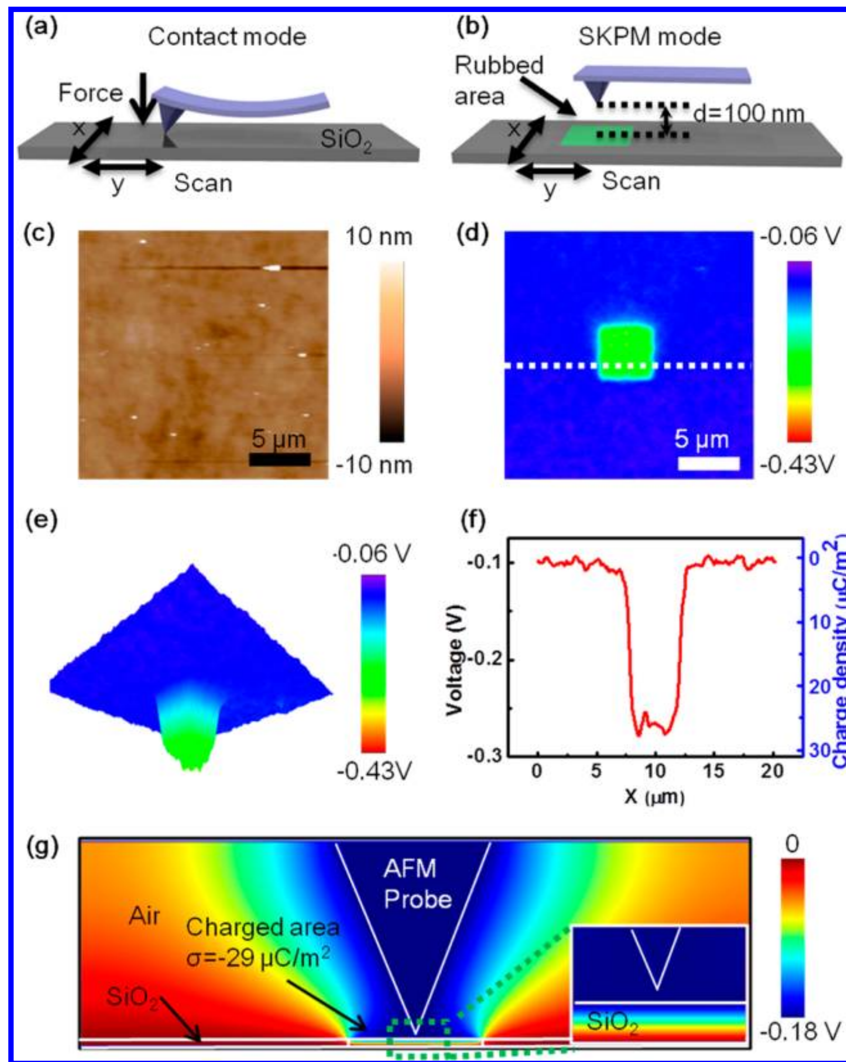

Figure 1. Schematic illustration of the experiments based on AFM. (a) Triboelectric charge generation by friction between AFM probe and SiO_2 and (b) subsequent surface potential characterization in the SKPM mode. (c) AFM topography of SKPM surface potential image. (d) AFM topography of a larger area on SiO_2. The dashed line corresponds to the profile in f. (e) 3D image of the measured surface potential profile. (f) Cross section profile of the potential distribution. (g) Simulated electric potential distribution in vertical direction under the condition when surface potential was measured in SKPM. Parameters used in simulation: the apex angle of the AFM probe was set to 35° with a tip radius of 10 nm, and had potential of −0.168 V; the center 4 μm area on top surface of SiO_2 had surface charges with a density of −29 $\mu C/m^2$, and the bottom surface of SiO_2 was grounded. The inset is an enlarged picture of the tip area.

potential of the rubbed area were characterized in situ in the scanning Kelvin potential microscopy (SKPM) mode (Figure 1b) with the underlying Si wafer grounded.[20−22] Positive and negative charges can be transferred to the SiO_2 surface through triboelectrification using Si-based probes with and without Pt coating, respectively. As shown in Figures 1c and d, there is no detectable topographic change but a clear contrast in the surface potential images between the rubbed and intact areas. Figure 1e illustrates the 3D potential distribution in a 20 × 20 μm^2 surface area. As shown from the cross section profile (Figure 1g), the potential of the rubbed area is 0.167 V lower than that of the intact area, suggesting that excess negative charges transferred by rubbing lowered the surface potential of the central area.

To quantify the triboelectric charge density, the relationship between the surface charge density and the measured potential from SKPM were investigated. The principle of the SKPM is to match the probe bias V_{DC} with the contact potential difference between the sample and the probe V_{CPD} by nullifying the vibration of the probe, which is initially driven by the electrostatic force F_{ES} induced on the AFM probe, as described in eq 1:[20]

$$F_{ES} = -\frac{\partial C_t}{\partial z}\left\{\frac{1}{2}\left[(V_{DC} - V_{CPD})^2 + \frac{1}{2}V_{AC}^2\right] + (V_{DC} - V_{CPD})V_{AC}\sin(\omega t) - \frac{1}{4}V_{AC}^2\cos(2\omega t)\right\} \quad (1)$$

where C_t, z, V_{AC}, and t are the equivalent capacitance between the tip and sample, the tip−sample distance, the magnitude of AC voltage applied to the probe, and the time, respectively.

The contact potential difference V_{CPD} is generally determined by two components: the effective work function of two materials and the electrostatic potential difference. The former component depends on the surface properties of the two materials, and the latter one is determined by the bias and surface charges of the sample.[20] Since the work function

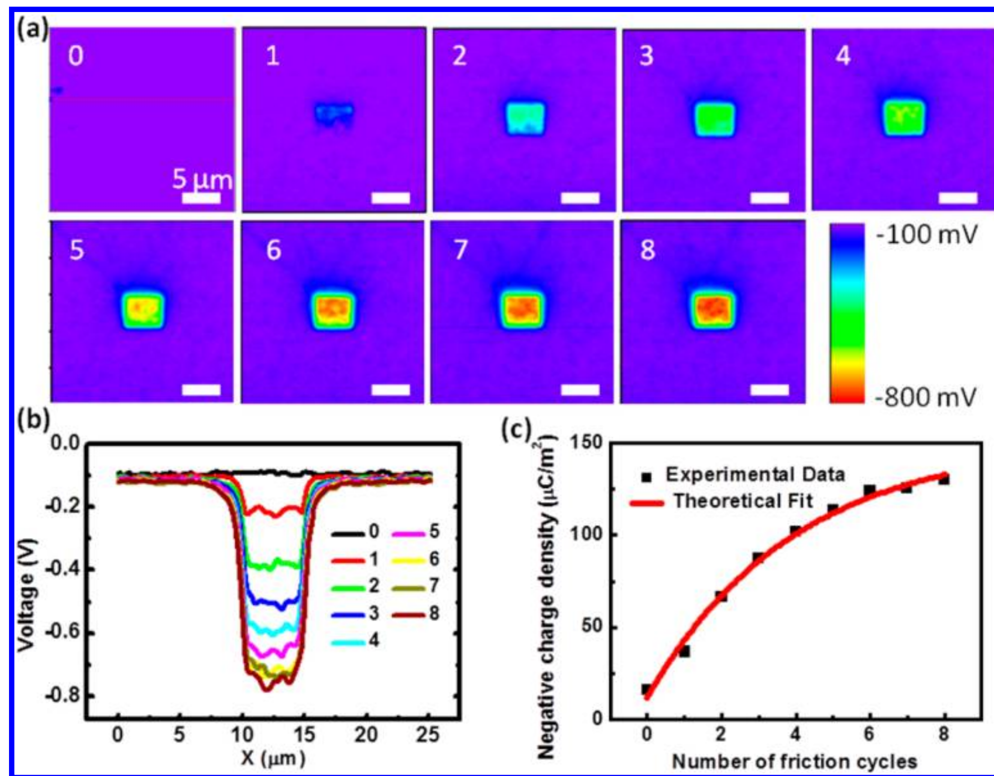

Figure 2. Triboelectric charge accumulation on the SiO_2 surface with the increase of the number of repeated rubbing at the same area. (a) Series of surface potential images taken in the same area from intact status to the one after 8th rubbing cycles and (b) their corresponding potential profiles. (c) Derived surface charge density as a function of the number of friction cycles and our fit based on charge accumulation theory described in eq 4.

difference is almost the same across the measured surface, the potential contrast between the rubbed area and the intact area ΔV should be determined by the triboelectric charge induced potential change. The charge induced SiO_2 surface potential change ΔV can be correlated to the surface charge density σ using a parallel capacitor model, as given in eq 2, since the scale of the charged area (4 μm) is much larger than the thickness of the SiO_2 film (200 nm).

$$\sigma = \frac{\Delta V \varepsilon_0 \varepsilon_{SiO_2}}{t_{SiO_2}} \tag{2}$$

where ε_0 is the vacuum dielectric constant and ε_{SiO_2} and t_{SiO_2} are the relative dielectric constant and thickness of SiO_2, respectively. In the case of $\Delta V = -0.167$ V, σ is calculated to be -29 $\mu C/m^2$. To verify the accuracy of the simplified model, we carried out a 2D numerical calculation for the potential distribution with the surface charge density of -29 $\mu C/m^2$ and the presence of the AFM probe. When the probe bias is set at -0.168 V, there is no potential gradient between the surface of charged area and the AFM probe, which indicates that the electrostatic force on the probe is nullified. This simulated bias value agrees very well with our measured -0.167 V.

Benefitting from the capability of controlled charge transferring and in situ measurement, the method as described above can be used to investigate the multifriction effect on the triboelectric charge transfer at the interface. In this experiment, the SiO_2 was rubbed for multiple cycles at the same area with constant contact force. The corresponding SKPM images after each friction cycle are shown in Figure 2a, and the extracted potential profiles are presented in Figure 2b. Within eight cycles of friction, the magnitude of the potential increased from 0.1 to 0.7 V at a slowing rate. To quantify this process, the surface charge density was calculated according to eq 2. As shown in Figure 2c, there is a clear trend for the surface charge accumulation and saturation process.

As in our experiment, the triboelectric process on the SiO_2 surface is considered as the cases of a metal−insulator. The mechanisms is mainly explained by the "effective work function" assumption in previous report, and the nature of the transfer can either be electron transfer, ion transfer, or even material transfer.[23,24] Regardless of the nature of the transfer, the amount of charges transferred in each contacting cycle is related to the difference in the effective work function of metal/semiconductor and the insulator, $\Delta\varphi$,[25] and the absolute value of $\Delta\varphi$ decreases with charge accumulating on the dielectric surface. When $\Delta\varphi = 0$, the triboelectric charges on the SiO_2 surface reach saturation. Thus, here we built a phenomenological model according to this proposed mechanism to fit our experimental result. Similar to the model for small particle charging,[26] the quantity of charges transferred each time is assumed to be proportional to the potential difference between the AFM probe and the SiO_2 surface. This potential difference consists of the work function difference between the two contacting materials V_c as well as the image charge potential V_e induced by existing charges on SiO_2 surface. V_c is a fixed value that only depends on material property, and V_e is proportional to the amount of existing charges.[26] Thus, the overall charge transfer in each cycle is described by eq 3

$$\frac{d\sigma}{dn} = kV_c - pV_e\sigma \tag{3}$$

where σ is the accumulated surface charge density, n is the number of friction cycles, k is considered as charging efficiency

dx.doi.org/10.1021/nl401006x | Nano Lett. XXXX, XXX, XXX−XXX

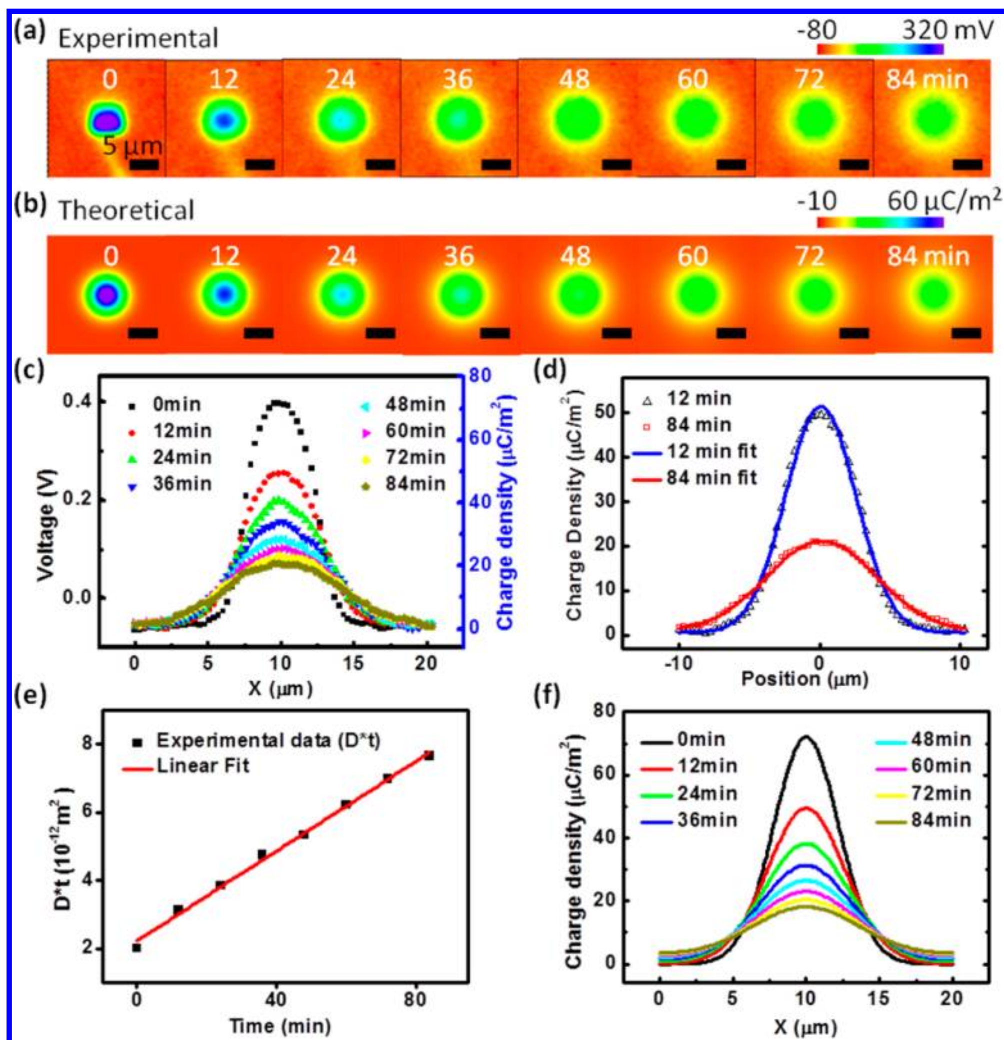

Figure 3. Charge diffusion over time. (a) Series of images of surface potential distribution as a function of time after the triboelectrification. (b) COMSOL simulation of surface charge density distribution. Initial charge density was set to be a Gaussian distribution: $4.5 \times 10^{14} \exp[-1.2 \times 10^{11}(x^2 + y^2)]$, and diffusion coefficient to be 1.10×10^{-15} m^2/s. (c) Cross sections of the series of images in a. (d) 1D Gaussian fit of the surface charge distribution at 12 min (blue) and 84 (red) min, respectively. The time constant (Dt) can be derived from this fitting. (e) Time constant at different time and its linear fitting. The slope indicates the diffusion coefficient. (f) The profiles of series of surface charge distribution images shown in b.

coefficient, and p is considered as charging impedance coefficient. The boundary condition for eq 3 is as follows: σ_0 is the surface charge density before triboelectric process (e.g., at $n = 0$), and σ_∞ the saturate charge density after infinite numbers of cycles of friction. The relationship between σ and n is then obtained as shown in eq 4.

$$\sigma = \sigma_0 \exp\left(-\frac{n}{n_0}\right) + \sigma_\infty\left\{1 - \exp\left(-\frac{n}{n_0}\right)\right\} \tag{4}$$

where $n_0 = 1/pV_e$ is the saturation constant that controls the speed of charge saturation, and $\sigma_\infty = kV_c/pV_e$. The equation fits the experimental data very well, as shown in Figure 2c. The constants were extracted from the fitting: $\sigma_0 = (-12 \pm 3)$ μC/m^2, $\sigma_\infty = (-150 \pm 8)$ μC/m^2, $n_0 = 3.9 \pm 0.5$. The adjusted R^2 of this fitting is 0.9911, suggesting a fairly good fit.

Similar charge accumulation behavior was also observed in the experiment of rubbing Pt coated probe on SiO_2 film (Supporting Information S1). The results and theoretical fit are included in Figure S1 of the Supporting Information. This quantitative model of charge accumulation with friction cycle paves the way for cycle controlled triboelectric charge transfer process.

In addition, taking advantage of the nanometer resolution of AFM and SKPM, the method is able to give insight on the migrating process of the triboelectric charges by monitoring the surface potential distribution within a time period after one cycle of triboelectrification. In our demonstrating experiment, an AFM tip first scanned over a 4×4 μm^2 area of SiO_2 surface in contact mode with a normal contact force of 120 nN to induce the triboelectric charges. The surface potential distribution was then monitored by SKPM every 12 min. Take the diffusion of the positive charge on SiO_2 rubbed by Pt tip as an example, as presented in Figure 3a, with time changing from 0 to 84 min, the charged area becomes larger, and the peak voltage contrast becomes smaller. From the profiles of the same cross section of each image as shown in Figure 3c, the peak of the potential decreases from 0.4 to −0.06 V, and the half width at full maximum of the potential distribution profile increases from 5.1 to 8.6 μm, indicating the diffusion of surface charges to adjacent area. Charges diffuse laterally on the surface in two dimensions as well as vertically into the bulk.[27] Here we

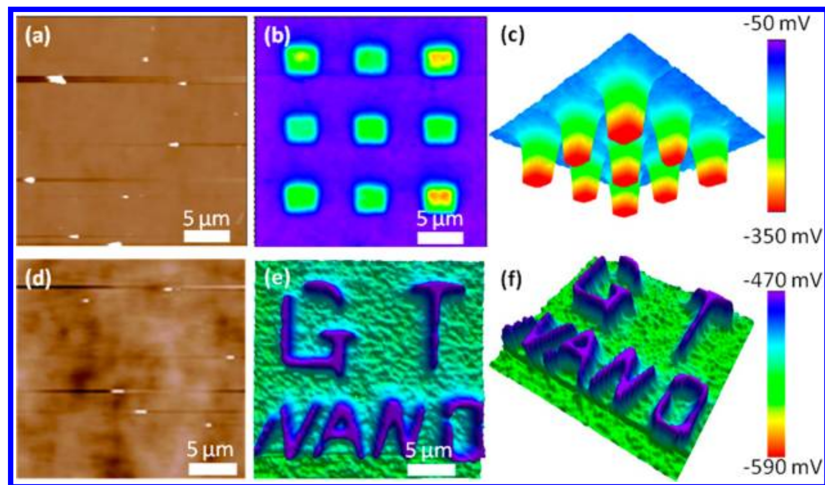

Figure 4. Patterning of the surface triboelectric charges on an insulator surface. Patterning of negative charges: (a) surface topography image and (b) 2D and (c) 3D images of charge density after patterning. Patterning of positive charges: (d) surface topography image and (e) top and (f) side views of 3D images of charge density after patterning.

assume that the surface diffusion rate is much higher than bulk diffusion. This is a reasonable approximation; otherwise most of the charges would have leaked into the bottom electrode rather than spreading over the surface because the characteristic length of the diffusion on the surface (about 3 μm) is much larger than the thickness of the SiO_2 (200 nm). Therefore, we employ the model for a two-dimensional diffusion to estimate the surface charge diffusion coefficient on SiO_2 on an unbounded uniform surface from a point source (x_0, y_0) from time t_0, as described in eq 5:[28]

$$\sigma(x, y, t) = \frac{A}{t - t_0}\exp\left[-\frac{(x - x_0)^2 + (y - y_0)^2}{4D(t - t_0)}\right] \quad (5)$$

where $\sigma(x, y, t)$ is the surface charge density of point (x, y) at time t, A is the magnitude constant, and D is the isotropic diffusion coefficient on the surface. To extract diffusion coefficient from experimental data by eq 5, each set of data at a cross section of $y = y_0$ at a specific time t_n was first fit with Gaussian distribution function $f_n(x)$:

$$f_n(x) = C_n \exp\left[-\frac{(x - x_0)^2}{2{w_n}^2}\right] \quad (6)$$

where C_n is the magnitude constant for $f_n(x)$ and w_n is the distribution width of the Gaussian function, as shown in Figure 3d. As a further analysis, comparing eq 6 with eq 5, the following relationship is revealed.

$$D(t_n - t_0) = \frac{1}{2}{w_n}^2 \quad (7)$$

By fitting the eight groups of data at different diffusing time (as illustrated in Figure 3c), a $1/2w^2$ vs t curve is given, where D is the slope of the curve. From the fitting, $D = (1.10 \pm 0.03) \times 10^{-15}$ m^2/s was obtained with $R^2 = 0.9953$. With this estimated diffusion coefficient, the charge distribution with time was simulated using the finite element method (COMSOL), as shown in Figures 3b and f, which matches very well to the experimental data. Using the same method, the negative surface charge diffusion coefficient on the SiO_2 was estimated to be $(0.19 \pm 0.01) \times 10^{-15}$ m^2/s (as shown in Figure S2 in the Supporting Information). The significant difference in the surface diffusion coefficients (more than 5 times higher for positive charges than for negative charges) may be related to difference in charge carriers and the structure of the surface.

With a precise position control, the AFM tip induced triboelectrification can also be used for patterning of surface charges at the nanoscale. The polarity of the written charges could be controlled by purposely choosing different probe materials. As demonstrated in Figure 4, both negative (a, b, and c) and positive charges (d, e, and f) can be written on the SiO_2 surface by using Si-based probes with and without Pt coating, respectively. The surface charges are successfully patterned, while the topography of the area was unchanged, which shows promising potential for directed self-assembly of charged nanostructures for nanoelectronic devices.[19]

In summary, we demonstrate an in situ method to quantitatively characterize the triboelectrification at nanoscale via a combination of contact mode atomic force microscopy (AFM) and scanning Kevin probe microscopy (SKPM). Using this method, we systematically investigated the in situ charge transfer, charge accumulation from multicycles of friction, and subsequent charge diffusion on the dielectric surface. The triboelectric charges accumulated from multifriction and eventually reached a saturated concentration. The saturated charge density is consistent with the values estimated from the analytical model of triboelectric nanogenerators in previous papers. The calculated diffusion coefficients of charges at ambient environment suggests that the charge decay time constant is about tens of minutes, which validates the assumption of TENG's design that charges can be held between two consecutive contacts. This methodology can be applied to study triboelectrification of different metal—dielectric/polymer material systems, thereby providing a powerful tool to investigate the parameters that are important in designing high performance TENGs. Finally, the surface charges are successfully patterned while the topography of the area was unchanged, which has promising potential application for directed self-assembly of charged nanostructures for nanoelectronic devices.

Methods. The experiments were conducted in a MFP-3D atomic force microscope (AFM) from Asylum Research at ambient environment with a relative humidity of 50%. The Si-based probe with Pt coating was AC240TM produced by

Olympus. The Si-based probe without Pt coating was prepared by mechanically wearing the Pt layer off the tip of the conductive probe (AC240TM from Olympus), where the probe was scanned on the sapphire under a contact force of 600 nN for three cycles. The SiO_2 layer of 200 nm in thickness was grown on an n-type silicon wafer through thermal oxidation. For charge generation, the AFM was working in contact mode, while the normal contact force was calculated from the product of inverse optical lever amplification (81.6 nm/V), deflection set point (0.1−2 V), and spring constant of the tip (1.46 N/m). For characterization of surface charges, the AFM was working in scanning Kelvin probe microscopy (SKPM) mode, while the tapping amplitude was set to be 560 mV and lift height to be 50 nm. The tip sample distance was determined by the summation of lift height and average tapping tip−sample distance, which was calculated as the product of dynamic optical lever sensitivity (88.9 nm/V) and tapping amplitude set point (0.56 V). Therefore, the tip-to-sample distance was 100 nm in the SKPM mode.

■ ASSOCIATED CONTENT

Supporting Information

Details about the multifriction effect on positive charge transfer and the charge diffusion experiment results for negative charges on SiO_2 surface are included. This material is available free of charge via the Internet at http://pubs.acs.org.

■ AUTHOR INFORMATION

Corresponding Author

*E-mail: zlwang@gatech.edu.

Author Contributions

Y.S.Z., Y.L., and G.Z. contributed equally to this work.

Notes

The authors declare no competing financial interest.

■ ACKNOWLEDGMENTS

Research was supported by U.S. Department of Energy, Office of Basic Energy Sciences (Award DE-FG02-07ER46394), NSF (0946418), and the Knowledge Innovation Program of the Chinese Academy of Science (Grant No. KJCX2-YW-M13). The authors thank R. Hinchet, S. Wang, S. Niu, K. Pradel, and S. Lee for fruitful discussions.

■ REFERENCES

(1) Horn, R. G.; Smith, D. T. *Science* **1992**, *256* (5055), 362−364.
(2) Horn, R. G.; Smith, D. T.; Grabbe, A. *Nature* **1993**, *366* (6454), 442−443.
(3) Harper, W. R. *Contact and frictional electrification*; Laplacian Press: Morgan Hill, CA, 1998; p 369.
(4) Bailey, A. G. *J. Electrostat.* **1998**, *45* (2), 85−120.
(5) Burland, D. M.; Schein, L. B. *Phys. Today* **1986**, *39* (5), 46−53.
(6) Pai, D. M.; Springett, B. E. *Rev. Mod. Phys.* **1993**, *65* (1), 163−211.
(7) Kwetkus, B. A. *Particul. Sci. Technol.* **1998**, *16* (1), 55−68.
(8) Fan, F. R.; Tian, Z. T.; Wang, Z. L. *Nano Energy* **2012**, *1* (2), 7.
(9) Zhu, G.; Pan, C. F.; Guo, W. X.; Chen, C. Y.; Zhou, Y. S.; Yu, R. M.; Wang, Z. L. *Nano Lett.* **2012**, *12* (9), 4960−4965.
(10) Wang, S. H.; Lin, L.; Wang, Z. L. *Nano Lett.* **2012**, *12* (12), 6339−6346.
(11) Zhu, G.; Lin, Z. H.; Jing, Q.; Bai, P.; Pan, C. F.; Yang, Y.; Zhou, Y. S.; Wang, Z. L. *Nano Lett.* **2013**, *13* (2), 7.
(12) Elsdon, R.; Mitchell, F. R. G. *J. Phys. D: Appl. Phys.* **1976**, *9* (10), 1445−1460.
(13) Wiles, J. A.; Grzybowski, B. A.; Winkleman, A.; Whitesides, G. M. *Anal. Chem.* **2003**, *75* (18), 4859−4867.
(14) Thomas, S. W.; Vella, S. L.; Kaufman, G. K.; Whitesides, G. M. *Angew. Chem., Int. Ed.* **2008**, *47* (35), 6654−6656.
(15) McCarty, L. S.; Whitesides, G. M. *Angew. Chem., Int. Ed.* **2008**, *47* (12), 2188−2207.
(16) Cole, J. J.; Barry, C. R.; Knuesel, R. J.; Wang, X. Y.; Jacobs, H. O. *Langmuir* **2011**, *27* (11), 7321−7329.
(17) Baytekin, H. T.; Baytekin, B.; Soh, S.; Grzybowski, B. A. *Angew. Chem., Int. Ed.* **2011**, *50* (30), 6766−6770.
(18) Baytekin, H. T.; Patashinski, A. Z.; Branicki, M.; Baytekin, B.; Soh, S.; Grzybowski, B. A. *Science* **2011**, *333* (6040), 308−312.
(19) Mesquida, P.; Stemmer, A. *Adv. Mater.* **2001**, *13* (18), 1395−1398.
(20) Melitz, W.; Shen, J.; Kummel, A. C.; Lee, S. *Surf. Sci. Rep.* **2011**, *66* (1), 1−27.
(21) Nonnenmacher, M.; Oboyle, M. P.; Wickramasinghe, H. K. *Appl. Phys. Lett.* **1991**, *58* (25), 2921−2923.
(22) Hong, J. W.; Park, S. I.; Khim, Z. G. *Rev. Sci. Instrum.* **1999**, *70* (3), 1735−1739.
(23) Williams, M. W. *Aip Adv.* **2012**, *2* (1), 010701.
(24) Matsusaka, S.; Maruyama, H.; Matsuyama, T.; Ghadiri, M. *Chem. Eng. Sci.* **2010**, *65* (22), 5781−5807.
(25) Cole, B. N.; Baum, M. R.; Mobbs, F. R. *Proc. Inst. Mech. Eng.* **1969**, *184* (3), 77−83.
(26) Matsusaka, S.; Ghadiri, M.; Masuda, H. *J. Phys. D: Appl. Phys.* **2000**, *33* (18), 2311−2319.
(27) Knorr, N.; Rosselli, S.; Nelles, G. *J. Appl. Phys.* **2010**, *107* (5), 054106.
(28) Guenther, R. B.; Lee, J. W. *Partial differential equations of mathematical physics and integral equations*; Dover Publications: New York, 1996; p 562.